A novel artificial neuron-like gas sensor constructed from CuS quantum dots/Bi_2S_3 nanosheets

Xinwei Chen[1], Tao Wang[1], Jia Shi[1], Shuyue Zheng[2], Wen Lv[1], Yutong Han[1], Min Zeng[1], Jianhua Yang[1], Nantao Hu[1], Yanjie Su[1], Hao Wei[1], Zhihua Zhou[1], Zhi Yang[1]*, Yafei Zhang[1]*

[1] Key Laboratory of Thin Film and Microfabrication (Ministry of Education), Department of Micro/Nano Electronics, Institute of Marine Equipment, School of Electronic Information and Electrical Engineering, Shanghai Jiao Tong University, Shanghai 200240, P. R. China.

[2] Department of Breast Surgery, Fudan University Shanghai Cancer Center, Shanghai 200032, P. R. China.

*Corresponding authors. E-mail address: zhiyang@sjtu.edu.cn and yfzhang@sjtu.edu.cn.

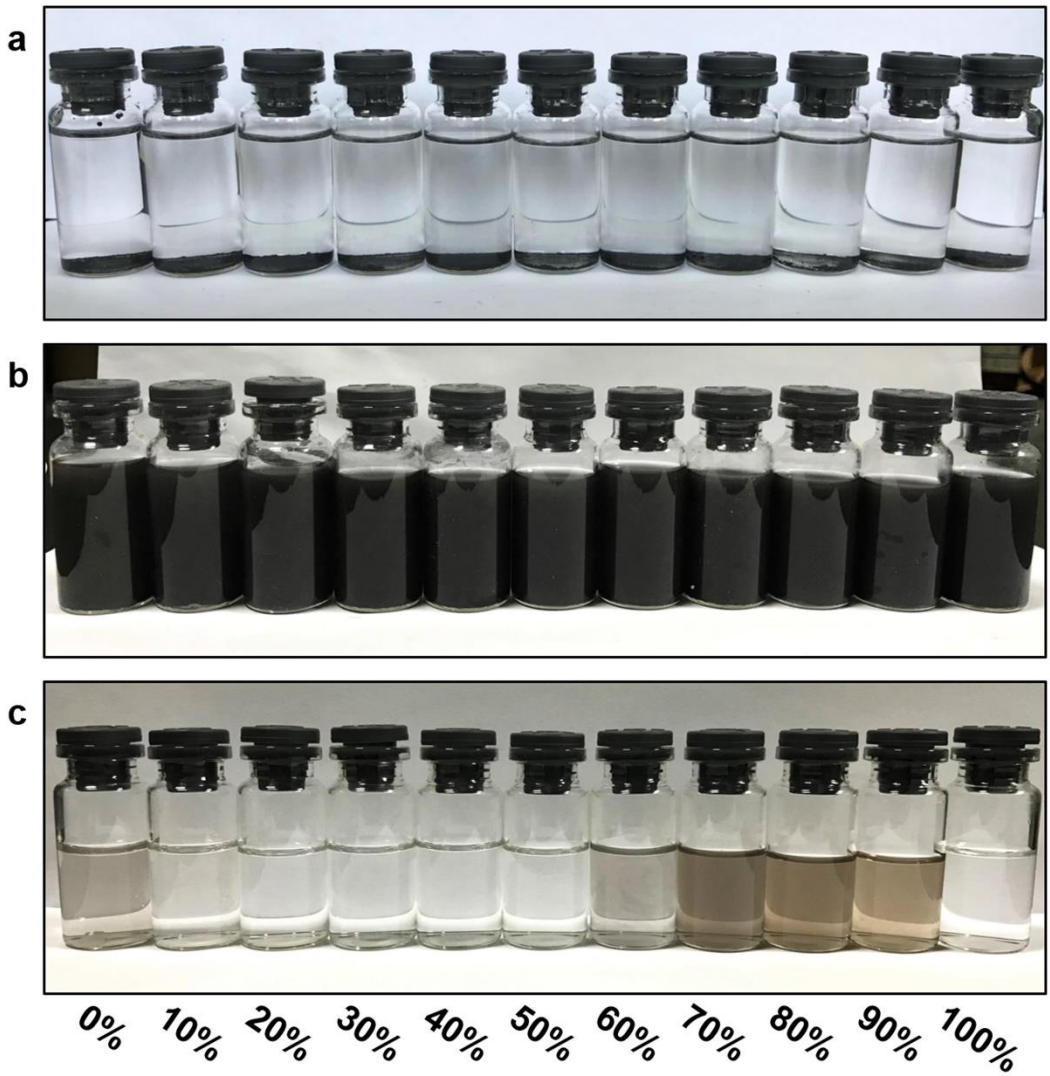

Fig. S1 Photographs of Bi_2S_3 dispersions in various ethanol/water mixtures: **a** Before and **b** after ultrasonication treatment for 8 h. **c** Supernatant collection by centrifugation at 3000 rpm.

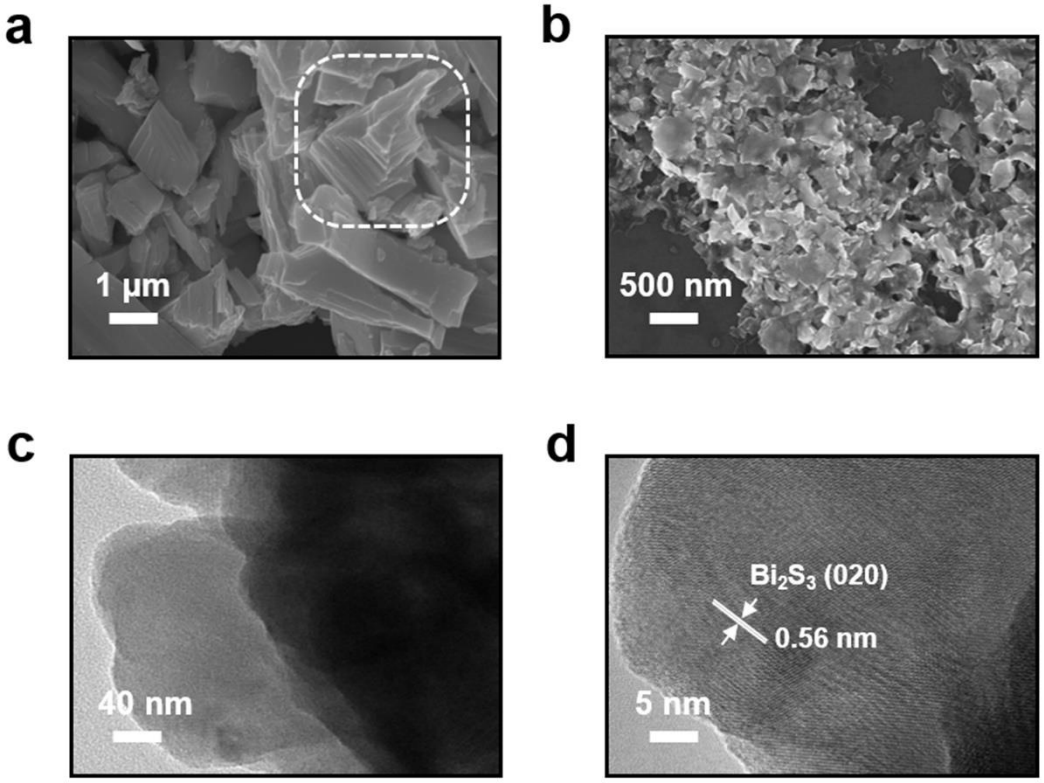

Fig. S2 SEM image of Bi_2S_3 samples before **a** and after **b** Liquid phase stripping. **c** and **d** TEM and HR-TEM images of Bi_2S_3 NSs.

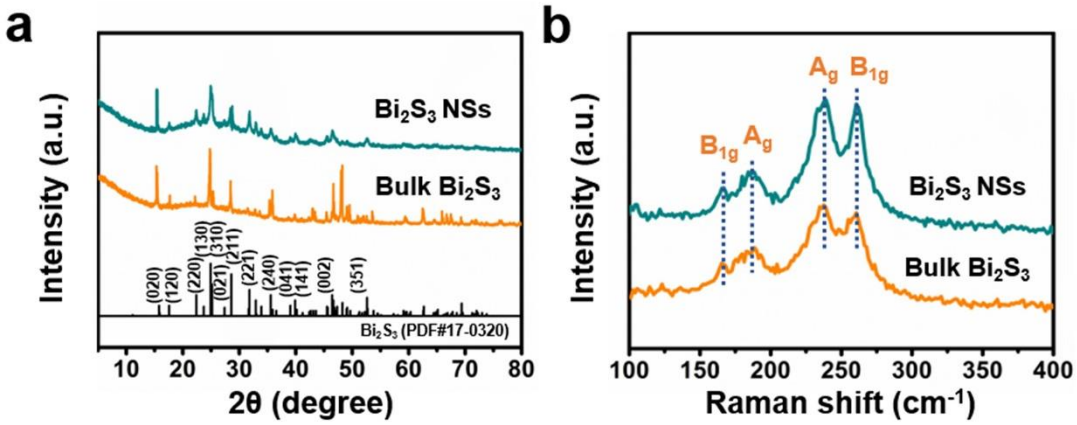

Fig. S3 XRD patterns **a** and Raman spectra **b** of bulk Bi_2S_3 and Bi_2S_3 NSs.

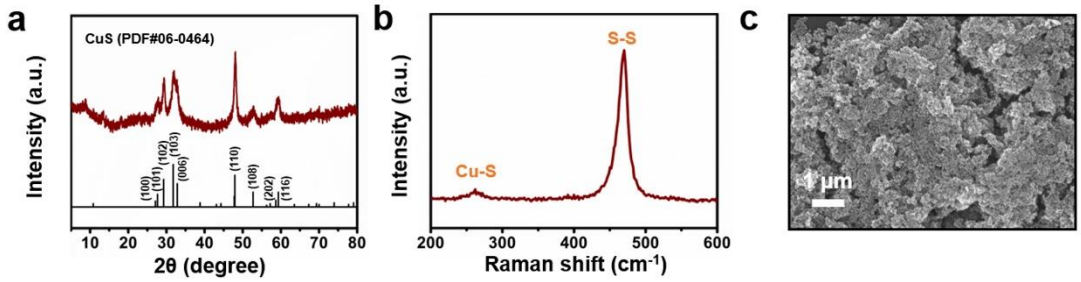

Fig. S4 a XRD pattern **b** Raman spectra and **c** SEM image of CuS sample.

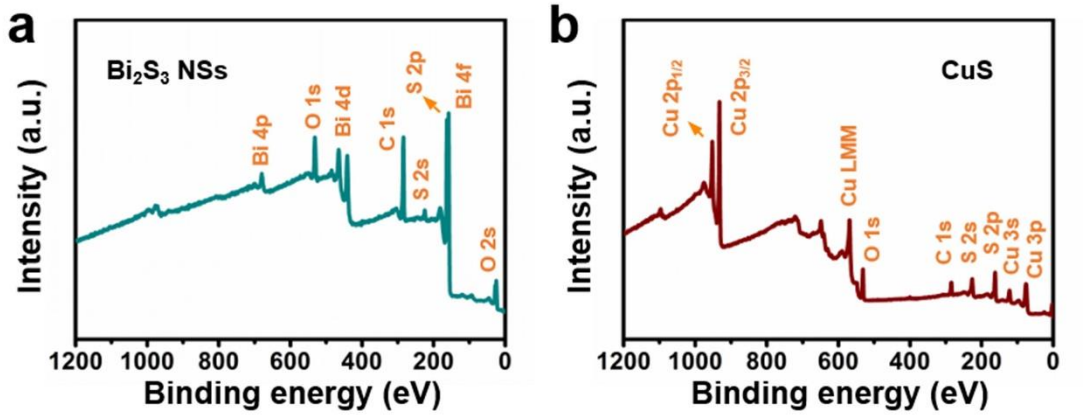

Fig. S5 Full XPS survey spectrums of **a** Bi_2S_3 NSs and **b** CuS.

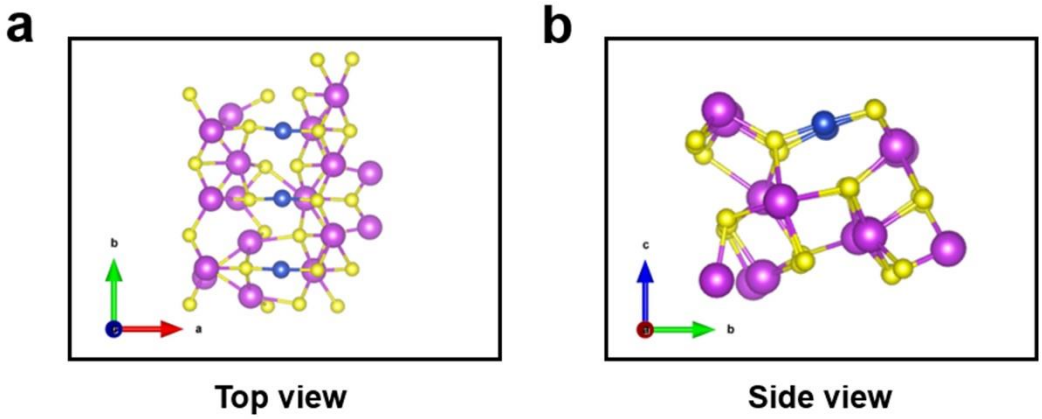

Fig. S6 The atomic structure of CuS-Bi_2S_3.

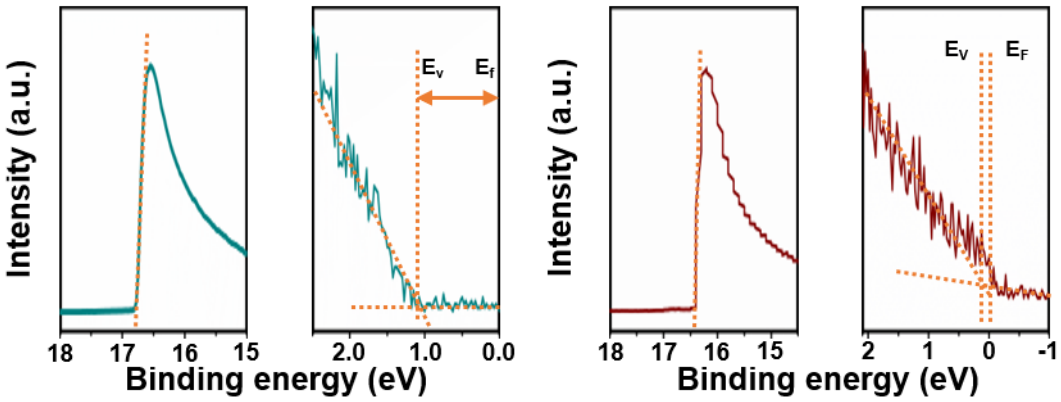

Fig. S7 UPS spectra of **a** Bi_2S_3 and **b** CuS: the secondary electron cut-off energy region (left) and low binding energy region (right) of each.

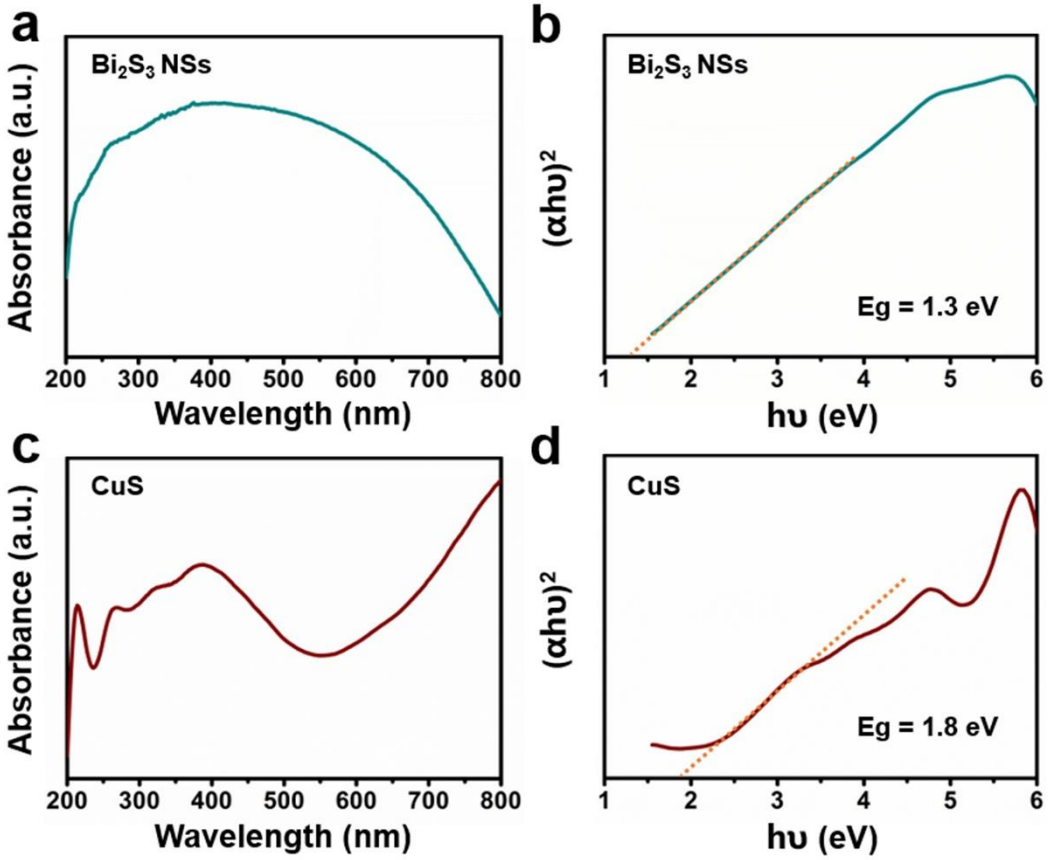

Fig. S8 UV−vis diffuse reflectance spectra of **a** Bi_2S_3 NSs and **c** CuS. $(\alpha h\nu)^2$ v.s. hν curve of **b** Bi_2S_3 NSs and **d** CuS.

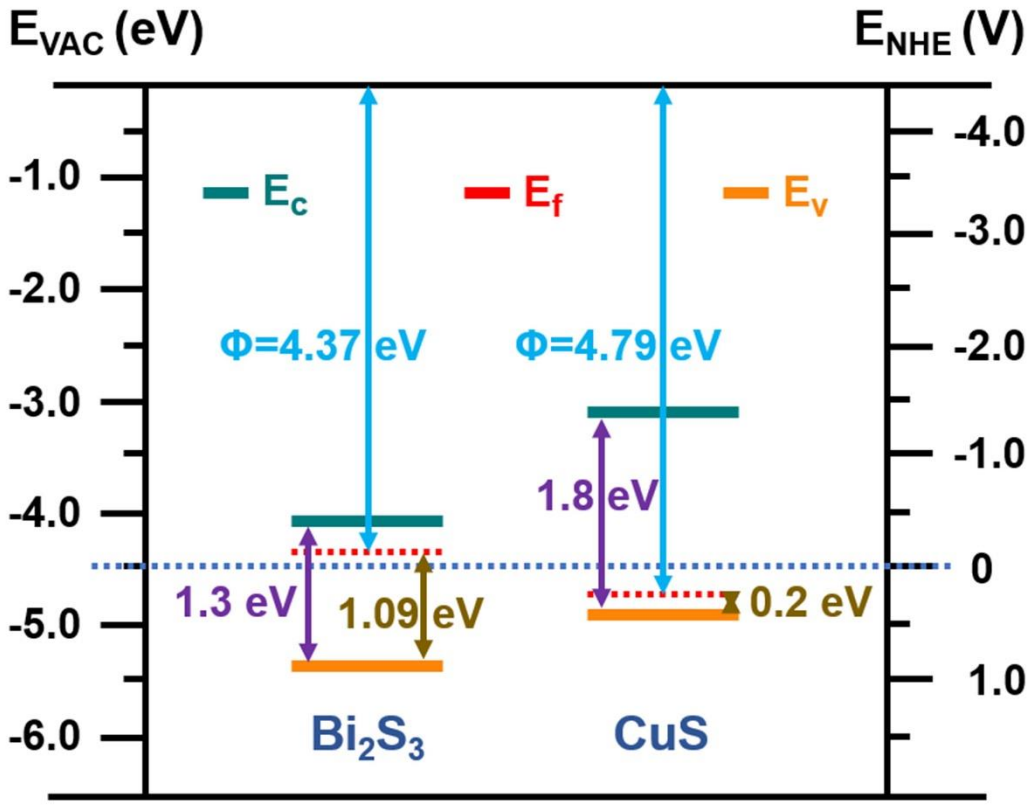

Fig. S9 Energy level diagram between interfacial materials CuS and Bi_2S_3 and schematic diagram of the charge transfer process.

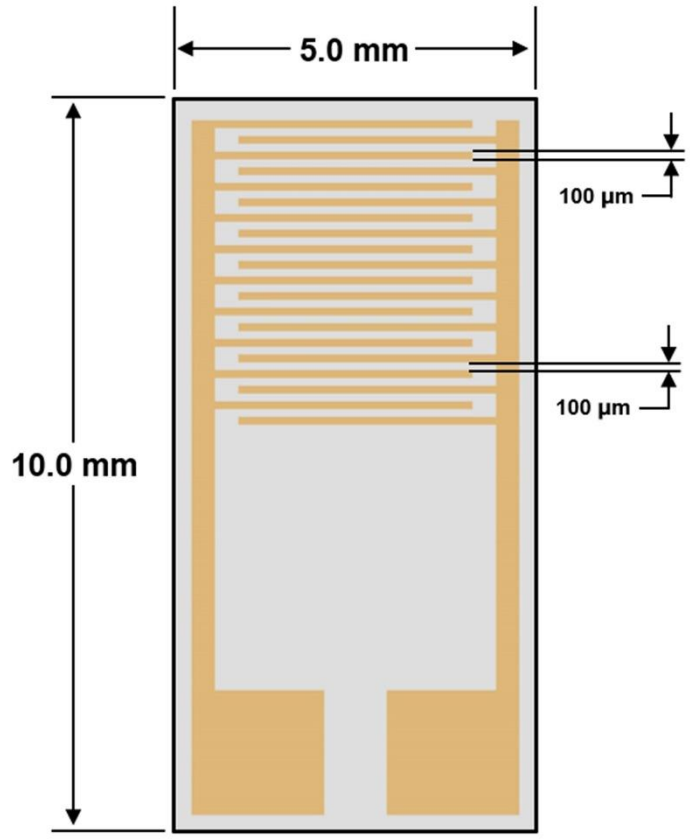

Fig. S10 Structure diagram of the flexible interdigital electrode.

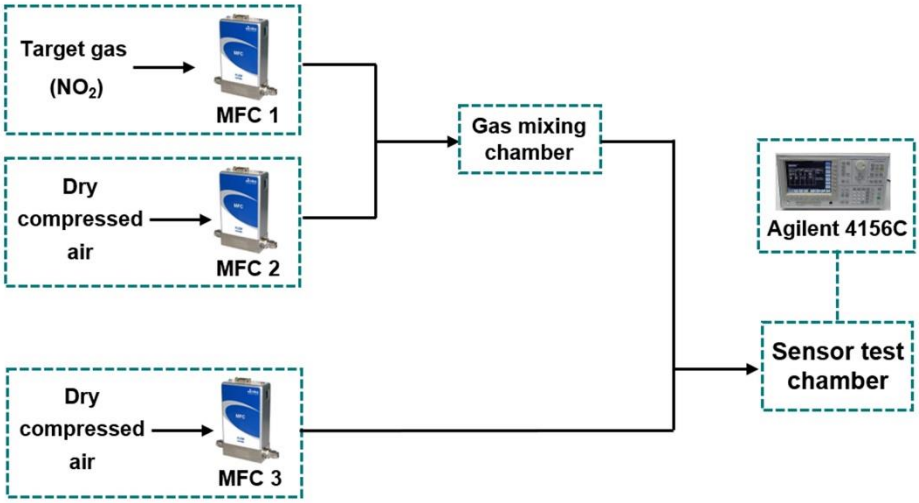

Fig. S11 Schematic diagram of the homemade gas-control system.

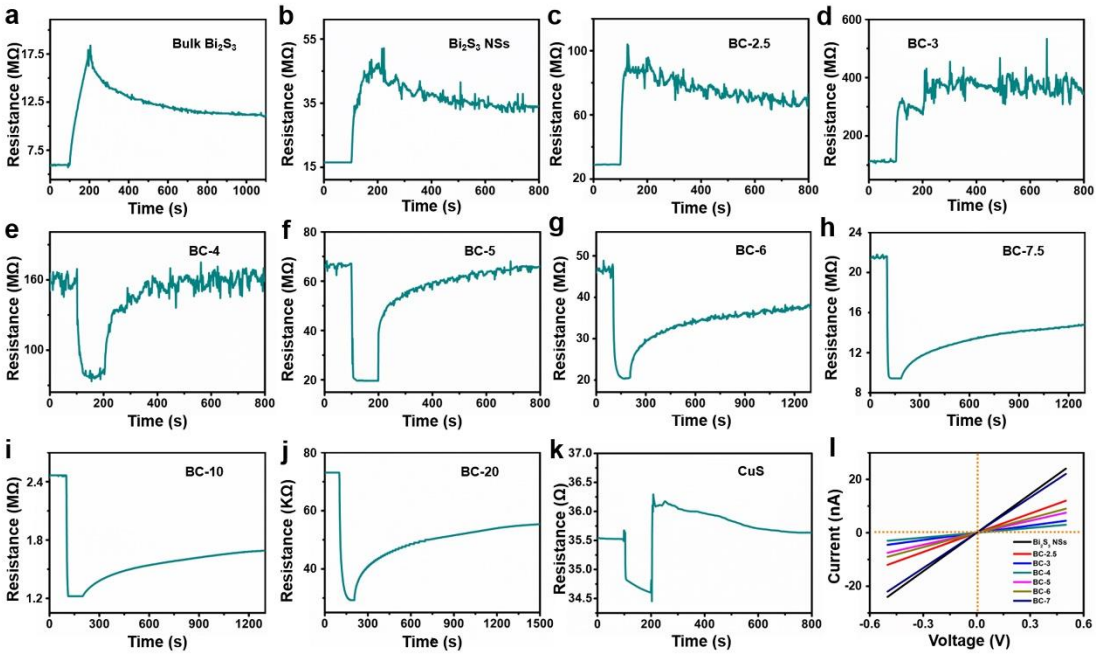

Fig. S12 a-k Sensitive response at a concentration to 10 ppm NO_2 through a dynamic gas-sensing room temperature testing for bulk pure Bi_2S_3, Bi_2S_3 NSs, BC-2.5, BC-3, BC-4, BC-5, BC-6, BC-7.5, BC-10, BC-20, and pure CuS. **l** *I-V* curves of Bi_2S_3, different content of CuS QDs/Bi_2S_3 NSs and CuS-based gas sensors.

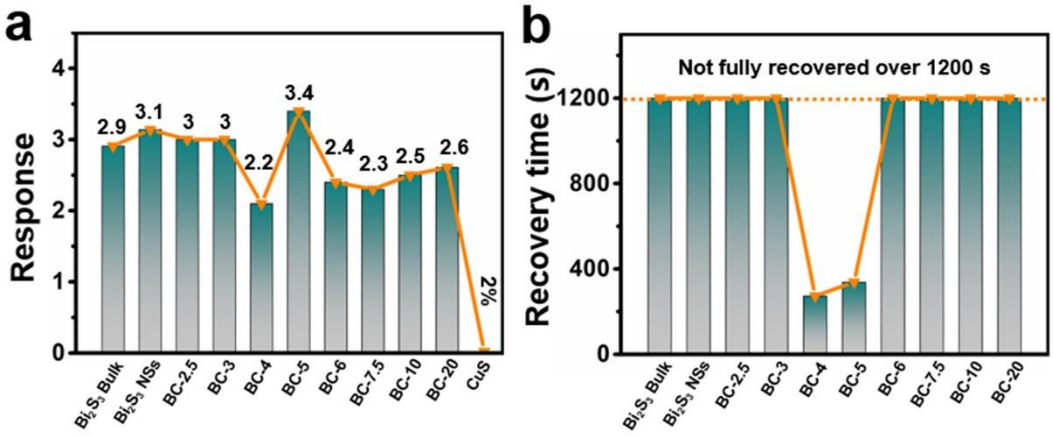

Fig. S13 a Response and **b** recovery performances of Bi_2S_3, different content of CuS QDs/Bi_2S_3 NSs, and CuS-based gas sensors to 10 ppm NO_2.

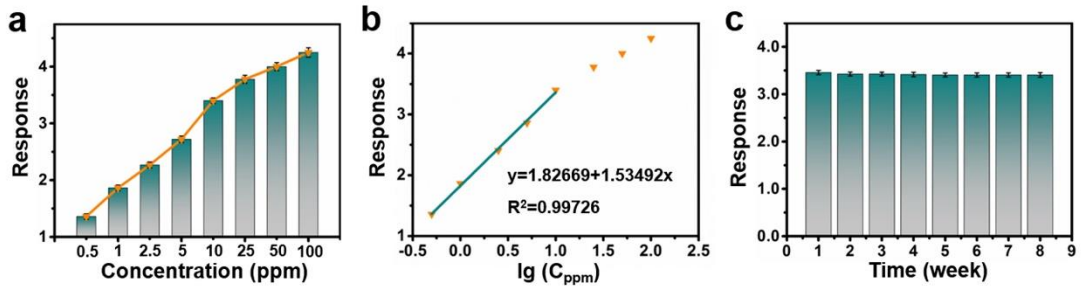

Fig. S14 a The response value of BC-5 sensor to different concentrations of NO_2 and its error bars. **b** The response of BC-5-based sensor as a function of the logarithm of the NO_2 concentration. **c** Long-term stability of BC-5-based sensor.

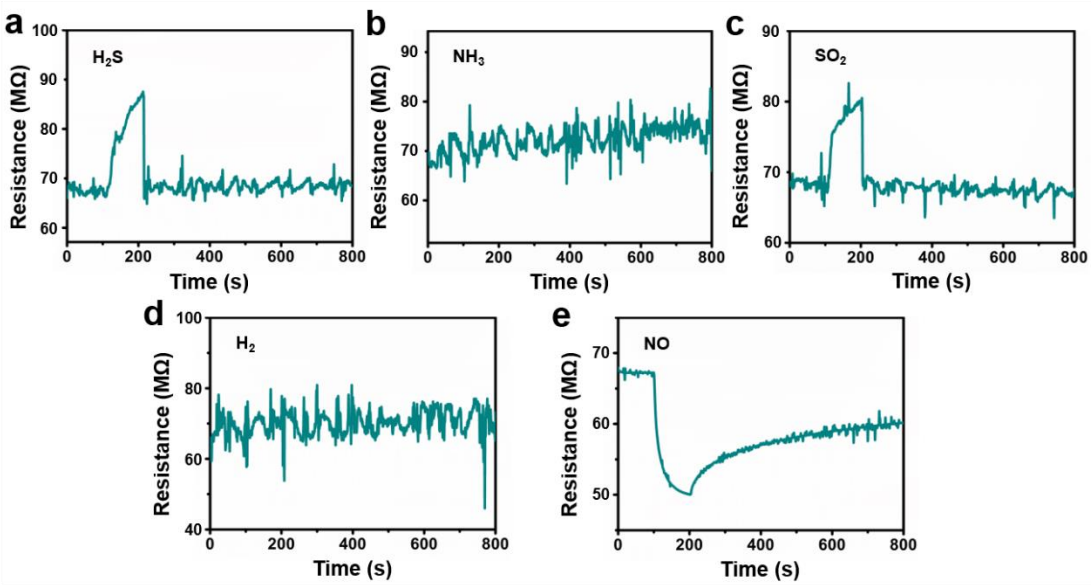

Fig. S15 The selectivity of the BC-5-based sensor to 10 ppm different target gases of **a** H_2S, **b** NH_3, **c** SO_2, **d** H_2 and **e** NO.

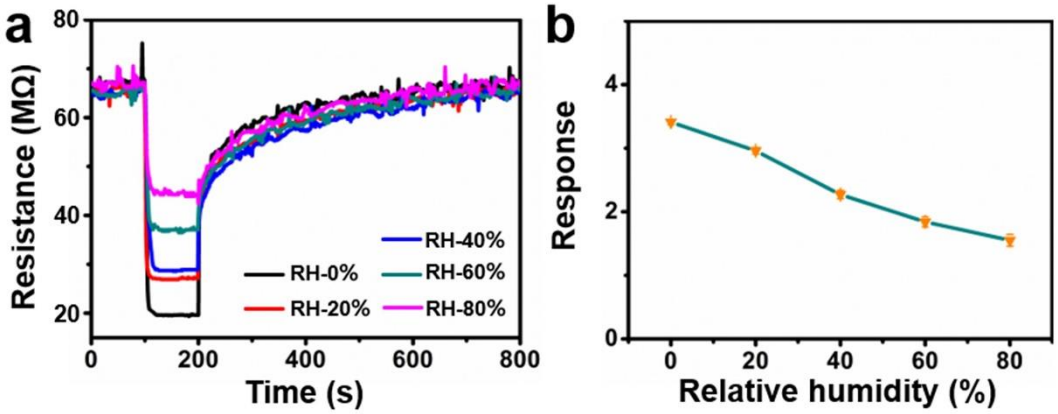

Fig. S16 Sensing characteristics of the sensor to 10 ppm NO_2 at different humidity levels.

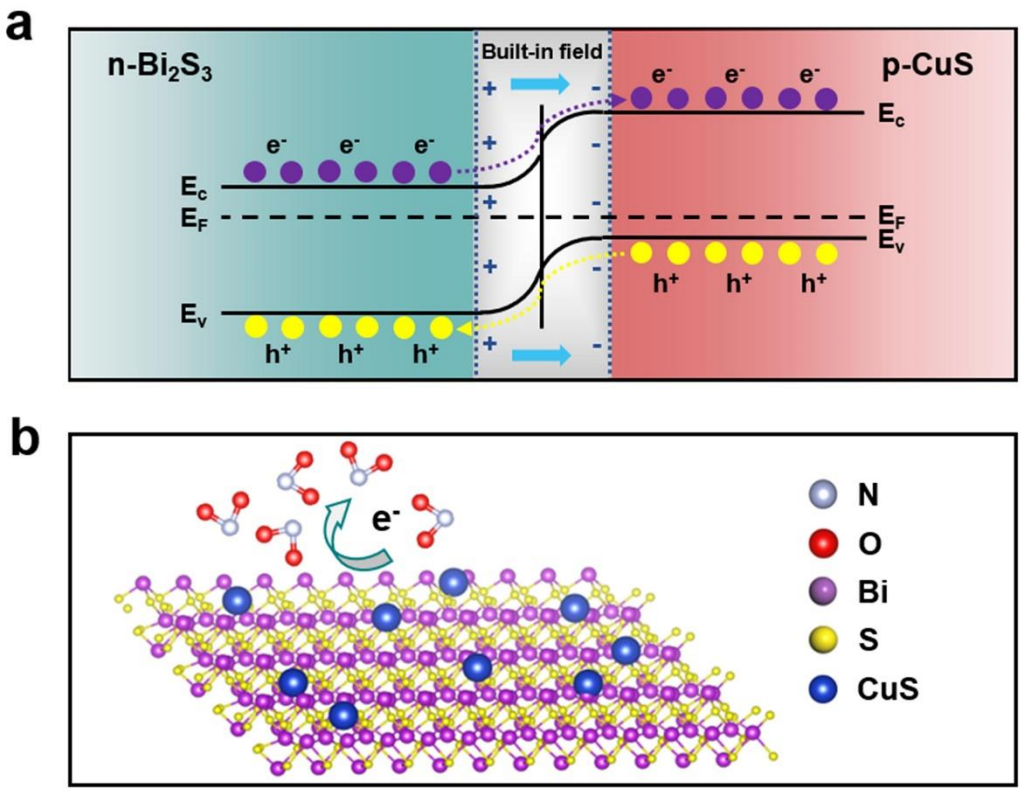

Fig. S17 a Energy band structures of CuS QDs/Bi_2S_3 NSs heterostructure in air. **b** the proposed sensing mechanism of the heterostructure.

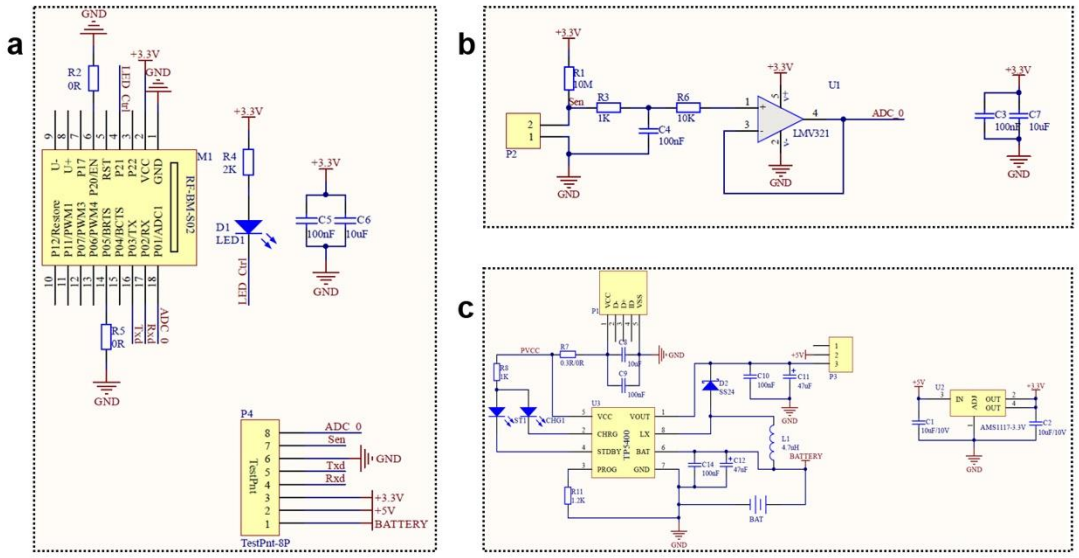

Fig. S18 The schematic circuit diagram of the flexible printed circuit board: **a** Data acquisition and communication circuit. **b** Sensor front-end circuit. **c** USB/Wireless charging circuit.

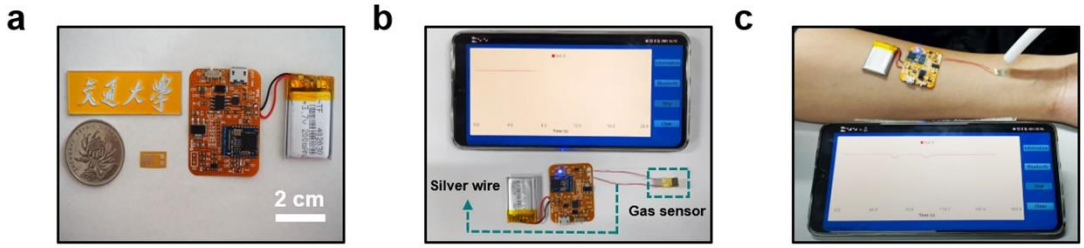

Fig. S19 a Photograph of the flexible circuit and electrode used in the current work (placed next to a school logo and 1 RMB coin for comparison). **b** Photographs of Bluetooth signal connection of wearable sensor device. **c** Photographs of wireless sensor signal acquisition process of the wearable sensor device.

Table S1 The bond length of M-O on NO_2-CuS-Bi_2S_3 structure.

Binding structure	Atoms	Bond	Length (Å)
n1	N (from NO_2)	Cu-N	1.978
	Cu (CuS-Bi_2S_3)		
n2	O (from NO_2)	Bi-O	2.025
	Bi (CuS-Bi_2S_3)		2.018
n3	O (from NO_2)	Cu-O	2.396
	Bi/Cu (CuS-Bi_2S_3)	Bi-O	2.557
n4	O (from NO_2)	Cu-O	2.555
	Cu (CuS-Bi_2S_3)		2.567

Table S2 The charge and charge transfer of NO_2 correlated to Fig. 5.

Binding structure	Atoms	Charge	Charge transfer
n2	N	4.4197582	-0.5802418
	O	6.5942103	0.5942103
	O	6.6273451	0.6273451
	Total-NO_2		0.6413136
n4	N	4.4885298	-0.5114702
	O	6.598587	0.598587
	O	6.6327922	0.6327922
	Total-NO_2		0.719909

Table S3 The charge and charge transfer of CuS correlated to Fig. 3d.

Binding structure	Atoms	Charge (e)	Charge transfer (e)
$CuS\text{-}Bi_2S_3$	Cu1	10.59286	-0.40714
	Cu2	10.59062	-0.40938
	Cu3	10.58872	-0.41128
	S1	6.800926	0.800926
	S2	6.751016	0.751016
	S3	6.768011	0.768011
	S4	6.763804	0.763804
	S5	6.771819	0.771819
	S6	6.74335	0.74335
	Total-CuS		3.371122

Table S4 Resistance values of bulk Bi_2S_3, Bi_2S_3 NSs, CuS, and different complex amounts of CuS QDs/Bi_2S_3 heterostructures.

	R		*R*
Bulk Bi_2S_3	6.4 MΩ	BC-6	48 MΩ
Bi_2S_3 NSs	17 MΩ	BC-7.5	21.5 MΩ
BC-2.5	30 MΩ	BC-10	2.5 MΩ
BC-3	110 MΩ	BC-20	73 KΩ
BC-4	160 MΩ	CuS	35.5 Ω
BC-5	66 MΩ		

Table S5 The room-temperature sensing performance comparison of NO_2 flexible gas sensors with different sensing materials.

Materials	Conc. (ppm)	Response	$\tau_{res.}$ (s)	$\tau_{rec.}$ (s)	LOD (ppb)	Ref.
$MoSe_2$	10	4 [a]	250	150	10	1
VA-2D MoS_2	5	380%[b]	500	Can't recover	-	2
SnS_2/S-rGO	1	75% [c]	600	1200	0.7	3
RGO/Mesoporous ZnO NSs	15	44% [c]	140	630	43.5	4
3D SnS_2-rGO	5	32.1% [d]	300	Can't recover	2.8	5
CuS QDs/Bi_2S_3	10	3.4 [e]	18	338	78	This work

Conc.: Gas concentration; Temp.: Operating temperature; $\tau_{rec.}$: Recovery time; RT: Room temperature.

[a] I_g/I_a.

[b] $\Delta I/I_0$

[c] $\Delta R/R_a$.

[d] $\Delta G/G$.

[e] R_g/R_a.

References

[1] S. Guo, D. Yang, S. Zhang, Q. Dong, B. Li, N. Tran, Z. Li, Y. Xiong, M.E. Zaghloul, Development of a cloud-based epidermal $MoSe_2$ device for hazardous gas sensing. Adv. Funct. Mater. **29**, 1900138 (2019). https://doi.org/10.1002/adfm.201900138

[2] M.A. Islam, H. Li, S. Moon, S.S. Han, H.-S. Chung, J. Ma, C. Yoo, T.-J. Ko, K.H. Oh, Y.J. Jung, Y.W. Jung, Vertically aligned 2D MoS_2 layers with strain-engineered serpentine patterns for high-performance stretchable gas sensors: experimental and theoretical demonstration. ACS Appl. Mater. Interfaces **12**(47), 53174−53183 (2020). https://doi.org/10.1021/acsami.0c17540

[3] Y. Huang, W. Jiao, Z. Chu, S. Wang, L. Chen, X. Nie, R. Wang, X. He, High sensitivity, humidity-independent, flexible NO_2 and NH_3 gas sensors based on SnS_2 hybrid functional graphene ink. ACS Appl. Mater. Interfaces **12**(1), 997−1004 (2020). https://doi.org/10.1021/acsami.9b14952

[4] W. Li, R. Chen, W. Qi, L. Cai, Y. Sun, M. Sun, C. Li, X. Yang, L. Xiang, D. Xie, T. Ren, Reduced graphene oxide/mesoporous ZnO NSs hybrid fibers for flexible, stretchable, twisted, and wearable NO_2 e-textile gas sensor. ACS Sens. **4**(10), 2809−2818 (2019). https://doi.org/10.1021/acssensors.9b01509

[5] J. Wu, Z. Wu, H. Ding, Y. Wei, W. Huang, X. Yang, Z. Li, L. Qiu, X. Wang, Three-dimensional graphene hydrogel decorated with SnO_2 for high-performance NO_2 sensing with enhanced immunity to humidity. ACS Appl. Mater. Interfaces **12**(2), 2634−2643 (2020). https://doi.org/10.1021/acsami.9b18098